# Surface-Structure-Assisted Chaotic Mode Lasing in Vertical Cavity Surface Emitting Lasers

Tsin-Dong Lee,[1] Chih-Yao Chen,[2] YuanYao Lin,[2] Ming-Chih Chou,[1] Te-ho Wu,[3] and Ray-Kuang Lee[2]

[1]*Graduate School of Optoelectronics, National Yunlin University of Science and Technology, Yunlin, 640 Taiwan*

[2]*Institute of Photonics Technologies, National Tsing-Hua University, Hsinchu, 300 Taiwan*

[3]*Graduate School of Material Sciences, National Yunlin University of Science and Technology, Yunlin, 640 Taiwan*

(Received 2 May 2008; published 22 August 2008)

We demonstrate chaotic mode lasing in vertical cavity surface emitting lasers at room temperature, with an open cavity confined laterally by the native oxide layer. Instead of introducing any defect mode, we show that suppression of lower-order cavity modes can be achieved by destroying vertical reflectors with a surface microstructure. Lasing on chaotic modes is observed directly through collecting near-field radiation patterns. Various vertical emission transverse modes are identified by the spectrum in experiments as well as numerical simulations in real and phase spaces.

DOI: 10.1103/PhysRevLett.101.084101 PACS numbers: 05.45.Mt, 42.55.Px, 42.65.Sf

Lasers are typically built with *integrable* cavity shapes to achieve a mirror reflectivity near unity. Based on circular symmetry in two dimensions, microdisk and microring semiconductor lasers have been introduced with the advantages of a small mode volume and a strong confinement [1]. Almost grazing incidence patterns confined by the total internal reflection at the interface, known as whispering-gallery (WG) modes of the electromagnetic field, lase in such stable resonators [2] and have attracted much attention in photonics, quantum electrodynamics, and telecommunications, due to their potential applications to modulate spontaneous emission and make thresholdless lasing. High-quality factor microdisks and microrings have been experimentally fabricated to demonstrate WG modes with embedded emitters based on compound semiconductor lasers [3,4], and more recently on silicon-on-insulator materials [5]. In the beginning, a waveguide is used to provide the confinement of light in the vertical direction for WG modes. With optical output vertically emitted from the surface, the vertical cavity surface emitting laser (VCSEL) is a natural choice for lasers with transverse behavior of a WG mode and a vertical emission [6].

Instead, *nonintegrable* and chaotic shapes of cavity can also support lasing modes. Once the shape of a resonator supports chaotic ray motions, localized eigenstates of the wave equation of electromagnetism, coined as scar modes [7,8], provide an alternative understanding in the correspondence between classical and quantum system [9,10]. In a fully chaotic cavity, there are no stable periodic orbits. An infinite number of unstable periodic orbits is needed to construct each wave function. Because of the correspondence between ray trajectories and optical modes, recently, deformed dielectric cavities with unstable periodic orbits constructed by a variety of shapes—asymmetric quadrupolar [7,11], stadium [12,13], and spiral-shaped microcavities [14]—have been demonstrated scar wave functions based on high-quality factor microdisk and microring lasers, in order to attack the fundamental issues and problems in quantum chaos and statistical mechanics. Along this direction, large area VCSELs have acted as an interesting billiard platform to demonstrate optical scar mode formation in mesoscopic system [15,16] by using cryogenic environments to suppress lower-order cavity modes.

In this Letter, a two-dimensional photonic crystal microstructure is fabricated on a VCSEL surface [17,18] to investigate the transverse optical pattern formation by directly collecting near-field radiation intensity. Instead of forming a defect cavity, we propose to use the surface structure as a deterioration mechanism for the desired lasing characteristics. As the whole vertical emission window of VCSEL is destroyed by the surface microstructure, we report the observation of higher-order WG-like modes confined laterally by the native oxide layer in a GaAs-based VCSEL. Through the suppression of lower-order cavity modes, chaotic mode lasing at room temperature is directly observed in experiments. The differences of threshold current and emission spectra between the same VCSEL with and without a surface microstructure are compared. Moreover, we show that by increasing the injection current, different vertical emission transverse patterns, corresponding to the superposition of modes at different wavelengths, are identified by using an electromagnetic wave field solver based on the finite element method and the Poincaré surface of section based on the ray trajectories in real and phase spaces, respectively. The experimental and numerical investigations in this work provide an effective state for investigating scar modes in microstructured semiconductor lasers.

The schematic diagram and scanning electron microscope (SEM) image of the microstructured VCSEL used in our experiments are shown in Fig. 1(a) and the inset in (b), respectively. The epitaxial layers of the VCSELs are grown by metal organic chemical vapor deposition (MOCVD) on a $n^+$-GaAs substrate, with graded-index separate confinement heterostructure (GRINSCH) active region formed by undoped triple-GaAs-AlGaAs quantum wells placed in one

 

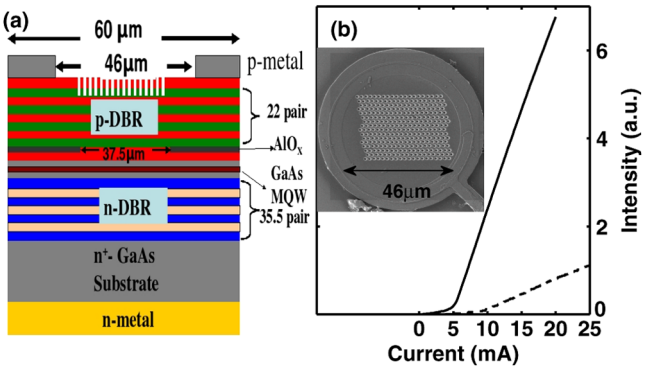


FIG. 1 (color online). (a) Schematic diagram and SEM image, inset in (b), of the device. (b) L-I curves for our VCSEL without (solid line) and with (dashed line) a surface microstructure.

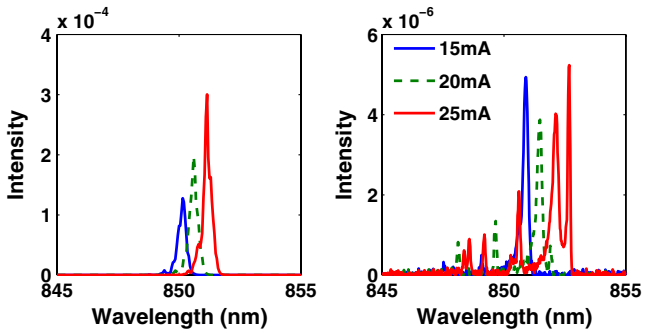


FIG. 2 (color online). The spectra of the VCSEL without (a) and with (b) a surface microstructure at different injection currents.

lambda cavity. The upper and bottom distributed Bragg reflectors (DBRs) in the vertical cavity consist of 22 and 35.5 pairs of $Al_{0.1}Ga_{0.9}As/Al_{0.9}Ga_{0.1}As$ layers, respectively. We introduce an oxide aperture to reduce the lateral optical loss and leakage current. Then reactive ion etch (RIE) is performed to define mesas with diameters of 68 $\mu$m, where the $Al_{0.98}Ga_{0.02}As$ layer within the $Al_{0.9}Ga_{0.1}As$ confinement layers is selectively oxidized to $AlO_x$. The oxidation depth is about 15 $\mu$m towards the center from the mesa edge so that the resulting oxide aperture is around 37.5 $\mu$m in diameter. The thickness of the oxide layer is about 300 Å (within a quarter-$\lambda$ layer, and $\lambda = 850$ nm). The $p$-contact ring with a inner diameter of 46 $\mu$m and a width of 7 $\mu$m is formed on the top of the $p$-contact layer. The $n$-contact is formed at the bottom of the $n$-GaAs substrate. Detail device parameters and lasing characteristics can be found in our previous publication on a similar VCSEL device but with different compound material [19].

As a comparison, the lasing characteristics of this VCSEL is measured before introducing any surface microstructures. Later on, the microstructured surface pattern is defined by the focused ion beam. A hexagonal lattice pattern without any defect is fabricated within the $p$-contact ring to introduce surface photonic crystal structures. The lattice constant and diameter for this hexagonal photonic-crystal-structured VCSEL is 2 and 1 $\mu$m, respectively. Moreover, the depth for the surrounding holes is only 0.2 $\mu$m in order to destroy the vertical reflector only, but not to introduce any photonic band-gap effect.

Figure 1(b) shows the L-I curve, light versus current, of the VCSEL without and with a photonic crystal structure on it. The threshold currents for lasing operation are about 5 mA and 10 mA before and after introducing the surface microstructure. The increment of the threshold current is expected since that there is no defect mode induced. After turning on, the emission spectra of our VCSEL without and with surface microstructures at different operation currents are shown in Fig. 2 for a comparison. Like a usual VCSEL without any surface structures, the main single-mode lasing peak in the spectrum for our microstructured VCSEL also has the same tendency to shift to longer wavelength as the change of the refractive index induced by the injection currents. But in contrast to unstructured VCSELs, significant side modes appear in the shorter wavelengths, as those observed in a typical WG laser.

Next, we measure the near-field electromagnetic intensity distribution at a fixed injection current by a charge-coupled device (CCD) camera through a standard microsope with a 100$X$ lens. The measured field intensity pattern is performed at different distances along the vertical direction: i.e., on the surface of the aperture and emission windows, respectively. While the VCSEL is operated below threshold, for example, at the current of 9 mA, it can be seen clearly in Fig. 3(a) that spontaneous emission pattern just reflects the lateral cavity defined by the native oxide layer in the VCSEL and the photonic crsytal surface structure within. The VCSEL is operated below the threshold condition now. And at the emission window, as shown in Fig. 3(e), we can see nothing but a uniform distribution of spontaneous emission pattern as a large area VCSEL [20]. It can be seen clearly that the native oxide layer forms a choatic transverse shape of cavity for our VCSEL. In this case, the designed surface photonic crystal structure has no effect on the lasing characteristics for only shallow holes are fabricated.

As the injection current increases, the VCSEL is operated above threshold and begins to lase. Owing to the destruction of top DBR reflector induced by the surface microstructure, lower-order cavity modes are suppressed and surrounding WG-like optical patterns have a chance to lase. In Figs. 3(b) and 3(f), operated at 15 mA a clear WG-like grazing patterns confined by the total internal reflection with multiple lobes in the azimuthal direction is directly observed at room temperature. When operated at higher current, i.e., 20 mA, in addition to the surrounding optical patterns at the interface scarlike patterns appear in the center region, as shown in Figs. 3(c) and 3(g). By increasing the current to 25 mA, a strongly localized field pattern is shown in the marked region in Figs. 3(d) and 3(h)

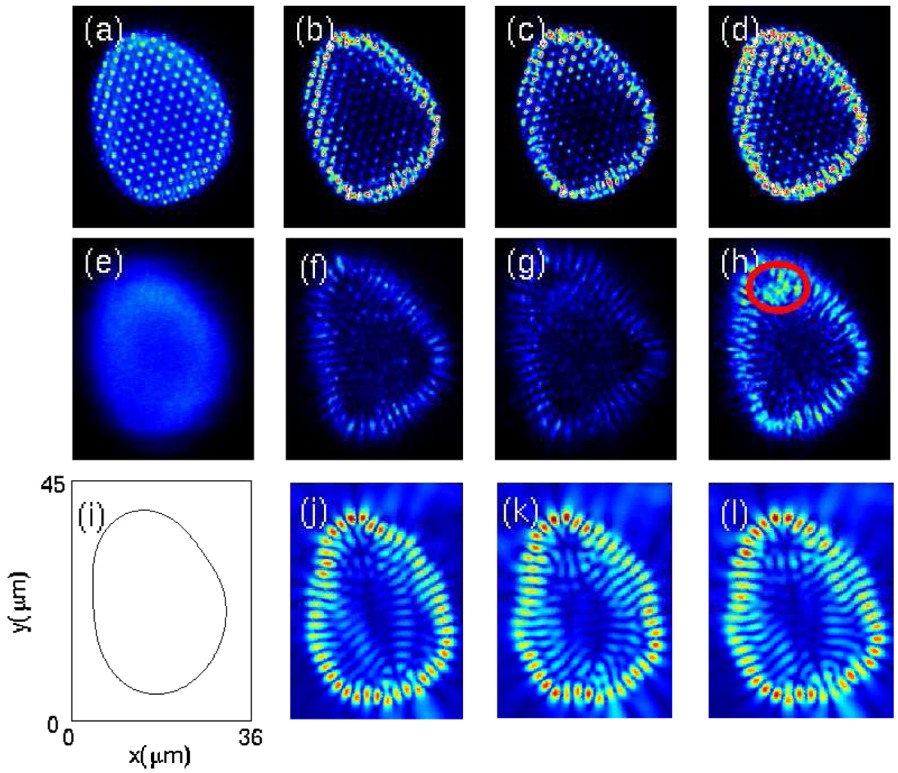


FIG. 3 (color online). Near-field intensity distributions on the surface of aperture (first row) and emission windows (second row) of our microstructured VCSEL at different injection currents, i.e., 9 mA (a),(e), 15 mA (b),(f), 20 mA (c),(g), and 25 mA (d),(h). Simulations of the field distribution (third row) of a surface structured VCSEL with the lateral boundary defined by an oxide layer (i) for the eigenmodes at wavelength of (j) 853.252, (k) 853.369, and (l) 853.374 nm, respectively.

. At this moment, the spectrum of emitting profile contains multiple lasing peaks, as shown in Fig. 2(b).

To illustrate the experimental observation of a chaotic mode lasing in such a defect-free microstructured VCSEL, we perform a two-dimensional mode solver based on the standard finite element method for electromagnetic waves to calculate the corresponding eigenmodes of this chaotic cavity [21]. Here due to the optical field confined by two DBR mirrors with the oxide layer of thickness about 300 Å that in the vertical direction, in this case we can safely reduce the 3D model into an effective 2D model by estimating the effective index. The lateral geometry defined by the native oxide layer is drawn according to the observed spontaneous emission pattern below the threshold current, as shown in Fig. 3(i). Then photonic crystal structures are embedded with the real lattice geometries. The effective refractive indices are assumed to be 1 in holes and 3.49 in the surrounding oxide layer. The calculated eigenmode (TE modes) for the wavelengths at 853.252 nm is shown in Fig. 3(j), which is a WG-like mode with the same number of lobes in the azimuthal direction as the experimental data. Figures 3(k) and 3(l) show the eigenmodes at wavelengths of 853.369 and 853.374 nm, with localized patterns in the center region. These nearly degenerate transverse eigenmodes modes result in a good agreement with the experimental observation in Fig. 3(h), and explain that one needs more than one eigenmode to construct the observed chaotic mode lasing in experiment.

Further, we perform the phase space analysis based on the ray trajectory to calculate the corresponding Poincaré section of surface [22,23]. The Birkoff coordinates are used as every time a ray collides with the cavity boundary at the arc length $s$ and the incidence angle $\chi$. Figure 4(a) shows the Poincaré section in the phase space of rays for the outer boundary of the native oxide layer in our VCSEL. As mentioned before, the photonic crystal surface structures are neglected in the ray trajectories for simplicity due to the fact that they play no major role in the lasing patterns in our experiments. As a comparison, in Fig. 4(b) we use a

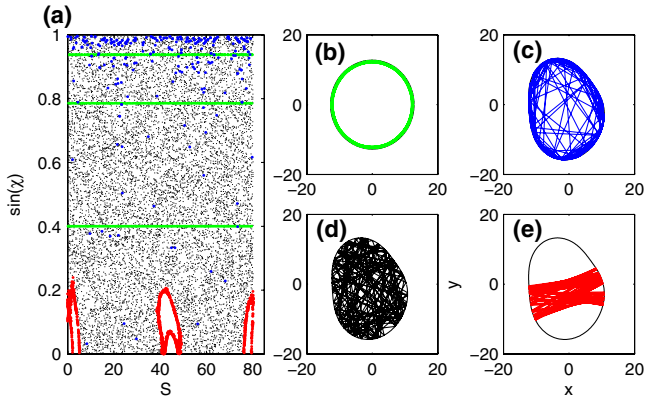


FIG. 4 (color online). (a) The Poincaré section of the surface for stable orbits for a stable cavity (green curves), fully chaotic motions in the native oxide defined cavity (black dots), short-lived periodic orbits (blue dots), and long-lived periodic orbit (red dots), with the axes of arc length, $s$, and the incident angle, $\sin(\chi)$. The corresponding patterns of ray motions are shown in (b)–(e) with the same colors.

circle shape with the same length of the circumference in our chaotic cavity to demonstrate stable periodic orbits (three green lines), i.e., WG orbits. For the observed oxide confined cavity, possible short-lived periodic orbit (blue dots) is found and shown in Fig. 4(c), which is very closed to the stable WG orbits and resembles the lasing mode observed in our experiments. These short-lived resonances named as chaotic WG modes have also been reported in chaotic microlasers [24,25]. Within the lifetime of our laser cavity, these chaotic WG modes have a chance to emit, even though in the long time scale the classical trajectories for our cavity occupied the whole Poincare section of the surface (black dots), as shown in Fig. 4(d). For the chaotic cavity in our VCSEL, we also find some long-lived periodic motions (red curves), with the trajectories shown in Fig. 4(e). But due to the condition of total internal reflections, only the ray motions in Fig. 4(c) have a high-quality factor to lase, which supports and explains the optical patterns demonstrated in our experiments above the threshold condition.

Before concluding, we discuss more about the difference between the chaotic mode lasing in a large area and our microstructured VCSELs. As pointed out previously, a cryogenic system is needed to suppress lower-order cavity modes in a large area VCSEL without performing any surface structure. But with surface structures, one can fabricate periodic (photonic-crystal-like) or random lattices inside the lasing area. Within a random medium, Anderson localization is well known to exist and demonstrated recently in photonic lattices [26]. In this work we only use the surface structure to destroy the vertical reflector without introducing band-gap effects in the transverse optical patterns, as shown in the experiments and confirmed by the numerical simulations. With a deeper depth of the surface holes in VCSELS, we believe that the microstructure VCSEL demonstrated here can provide an universal platform for studying chaotic and random systems. Conversely, our work will also interest the quantum chaos community, such as the transport of electrons in resonant tunneling diodes, for example, via donor impurities in tunnel diodes [27].

In conclusion, with microstructure patterns and near-field technologies we investigate the formation of transverse optical patterns in GaAs-based VCSELs. Without introducing any defect mode, the shallow surface structure is used to ruin the vertical reflector for the lower-order cavity modes. At the expense of higher threshold current, a native oxide laterally confined chaotic mode lasing in VCSELs can be directly observed at room temperature, by collecting the near-field intensity on the surfaces of aperture and emission windows. The observed different lasing modes, including WG-like and chaotic modes, are identified with numerical simulations in real and phase spaces. The experimental observations and the simulation results provide an alternative but effective approach to access chaotic modes in VCSELs at room temperature.

The authors are indebted to H. P. D. Yang for providing the samples, K. F. Huang and C.-H. Chang for useful discussions. This work is partly supported by the National Science Council of Taiwan with contrasts NSC 95-2112-M-224-001, NSC 96-2112-M-224-001, NSC 95-2112-M-007-058-MY3 and NSC 95-2120-M-001-006.

[1] *Optical microcavities*, edited by K. Vahala (World Scientific, Singapore, 2004).
[2] A. B. Matsko and V. S. Ilchenko, IEEE J. Sel. Top. Quantum Electron. **12**, 3 (2006).
[3] S. L. McCall *et al.*, Appl. Phys. Lett. **60**, 289 (1992).
[4] T. D. Lee *et al.*, Appl. Phys. Lett. **72**, 2223 (1998).
[5] J. S. Xia *et al.*, Appl. Phys. Lett. **90**, 141102 (2007).
[6] H. Soda *et al.*, Jpn. J. Appl. Phys. **18**, 2329 (1979).
[7] J. U. Nockel and A. D. Stone, Nature (London) **385**, 45 (1997).
[8] C. Gmachl *et al.*, Science **280**, 1556 (1998).
[9] E. J. Heller, Phys. Rev. Lett. **53**, 1515 (1984).
[10] M. C. Gutzwiller, *Chaos and Quantum Physics* (Springer-Verlag, New York, 1990).
[11] S.-B. Lee *et al.*, Phys. Rev. Lett. **88**, 033903 (2002).
[12] T. Harayama *et al.*, Phys. Rev. E **67**, 015207(R) (2003).
[13] W. Fang *et al.*, Phys. Rev. A **72**, 023815 (2005).
[14] S.-Y. Lee *et al.*, Phys. Rev. Lett. **93**, 164102 (2004).
[15] K. F. Huang *et al.*, Phys. Rev. Lett. **89**, 224102 (2002).
[16] T. Gensty *et al.*, Phys. Rev. Lett. **94**, 233901 (2005).
[17] T. Baba, IEEE J. Sel. Top. Quantum Electron. **3**, 808 (1997).
[18] O. Painter *et al.*, Science **284**, 1819 (1999).
[19] H. P. D. Yang *et al.*, Jpn. J. Appl. Phys. **46**, L509 (2007).
[20] H. Deng *et al.*, Appl. Phys. Lett. **69**, 3120 (1996).
[21] D. D. de Menezes *et al.*, Chaos **17**, 023116 (2007).
[22] K. Husimi, Proc. Phys. Math. Soc. Jpn. **22**, 264 (1940).
[23] M. Hentschel *et al.*, Europhys. Lett. **62**, 636 (2003).
[24] S. Chang *et al.*, J. Opt. Soc. Am. B **17**, 1828 (2000).
[25] V. P. Podolskiy *et al.*, Proc. Natl. Acad. Sci. U.S.A. **101**, 10 498 (2004).
[26] T. Schwartz *et al.*, Nature (London) **446**, 52 (2007).
[27] T. M. Fromhold *et al.*, Chaos Solitons Fractals **8**, 1381 (1997).